Research Article

Effects of delayed repair of peripheral nerve injury on the spatial distribution of motor endplates in target muscle

https://doi.org/10.4103/1673-5374.317990

Date of submission: January 24, 2021

Date of decision: March 15, 2021

Date of acceptance: April 21, 2021

Date of web publication: July 8, 2021

Dong-Dong Li[1, 2, #], Jin Deng[1, #], Bo Jin[1], Shuai Han[1], Xin-Yi Gu[1], Xue-Feng Zhou[2, *], Xiao-Feng Yin[1, *]

Graphical Abstract *Three-dimensional distribution of motor endplates (MEPs) in skeletal muscle after peripheral nerve injury and delayed reinnervation*

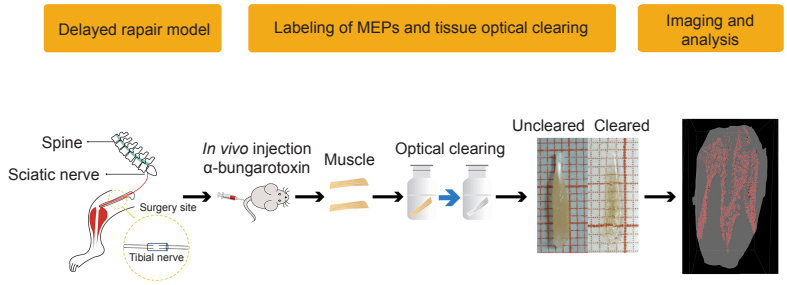

Abstract

Motor endplates (MEPs) are important sites of information exchange between motor neurons and skeletal muscle, and are distributed in an organized pattern of lamellae in the muscle. Delayed repair of peripheral nerve injury typically results in unsatisfactory functional recovery because of MEP degeneration. In this study, the mouse tibial nerve was transected and repaired with a biodegradable chitin conduit, immediately following or 1 or 3 months after the injury. Fluorescent α-bungarotoxin was injected to label MEPs. Tissue optical clearing combined with light-sheet microscopy revealed that MEPs were distributed in an organized pattern of lamellae in skeletal muscle after delayed repair for 1 and 3 months. However, the total number of MEPs, the number of MEPs per lamellar cluster, and the maturation of single MEPs in gastrocnemius muscle gradually decreased with increasing denervation time. These findings suggest that delayed repair can restore the spatial distribution of MEPs, but it has an adverse effect on the homogeneity of MEPs in the lamellar clusters and the total number of MEPs in the target muscle. The study procedures were approved by the Animal Ethics Committee of the Peking University People's Hospital (approval No. 2019PHC015) on April 8, 2019.

Key Words: degeneration; delayed repair; lamellar cluster; light-sheet microscopy; motor endplates; peripheral nerve injury; three-dimensional distribution; tissue optical clearing

Chinese Library Classification No. R444; R745; R337

Introduction

Peripheral nerve injury (PNI) is a common clinical condition. Because of the long distance between the target muscle and lesion site, delay in nerve repair, and the slow regeneration rate of the injured axons, it is difficult to effectively reconnect motor nerves with their target muscles in the clinical setting (Pisciotta et al., 2020; Zhang et al., 2021). With prolongation of denervation time, motor endplates (MEPs) progressively degenerate (Kobayashi et al., 1997; Höke, 2006), losing the capacity for information exchange between motor neurons and muscle fibers.

MEPs are important sites where motor neurons transform electrophysiological signals into chemical signals to control skeletal muscle activity. As neuromuscular junctions mature, acetylcholine receptor (AChR) clusters become perforated and complex, resembling pretzels with arrays or branches that are innervated by one axon per neuromuscular junction (Li et al., 2018). MEPs consist of AChRs possessing a high metabolic stability (half-life ≈ 10 days), and are induced and maintained by innervations (Bezakova et al., 2001). Muscle activity and lipid rafts also play important roles in maintaining the metabolic stability of AChRs (Rotzler et al., 1991; Bryndina et al., 2018). However, the AChRs become unstable (half-life ≈ 1 day) in denervated muscles after nerve injury because of denervation, loss of muscle activity, and perturbed lipid metabolism (Chao et al., 2013). The unstable AChRs impair the structural integrity of MEPs. AChR clusters gradually fragment and spread over a larger area without innervation after PNI (Magill et al., 2007; Slater, 2020). Changes in the morphology

[1]Department of Trauma and Orthopedics, Peking University People's Hospital, Beijing, China; [2]Department of Orthopedics, PLA Strategic Support Force Medical Center, Beijing, China

*Correspondence to: Xiao-Feng Yin, PhD, xiaofengyin@bjmu.edu.cn; Xue-Feng Zhou, zhouxuefeng306@sina.com.

https://orcid.org/0000-0001-9932-642X (Xiao-Feng Yin): https://orcid.org/0000-0002-6678-216X (Xue-Feng Zhou)

#Both authors contributed equally to the work.

Funding: *This study was supported by the National Natural Science Foundation of China, Nos. 82072162 (to XFY), 81971177; and the Natural Science Foundation of Beijing of China, No. 7192215 (to XFY).*

How to cite this article: *Li DD, Deng J, Jin B, Han S, Gu XY, Zhou XF, Yin XF (2022) Effects of delayed repair of peripheral nerve injury on the spatial distribution of motor endplates in target muscle. Neural Regen Res 17(2):459-464.*

of MEPs adversely affect the recovery of motor function (Sleigh et al., 2014a, b). Previous studies have investigated morphological and functional changes in single MEPs after PNI (Sleigh et al., 2014a; Slater, 2020).

Using tissue optical clearing methods, our recent studies (Chen et al., 2016; Yin et al., 2019) focused on the spatial distribution of MEPs in intact muscle. We showed that MEPs in skeletal muscles are distributed in an organized pattern of lamellar clusters. The MEPs are concentrated around thin-layer areas (i.e., lamellar clusters) in skeletal muscles. Each skeletal muscle has one or more distinctive MEP lamellar cluster. Based on the lamellar cluster, the intact muscle can be divided into one or more independent contractile units. We showed that the spatial distribution of MEPs is a key factor for the contraction of skeletal muscle. However, because of the limitations of the labeling and imaging methods for MEPs, the change in the spatial distribution of MEPs in intact skeletal muscle after delayed repair remained unknown. Therefore, in this study, we investigate the effects of delayed repair on the three-dimensional distribution of MEPs after PNI.

Materials and Methods

Animals

Forty-two female wild-type C57BL/6J mice (weighing 22–25 g, aged 6–8 weeks), bred in the Laboratory Animal Centre of Peking University People's Hospital (animal use license No. SYXK (Jing) 2016-0009), were used in the study. The study procedures were approved by the Animal ethics Committee of the Peking University People's Hospital (approval No. 2019PHC015) on April 8, 2019. All experiments complied with the ARRIVE guidelines, and were carried out in accordance with the National Institutes of Health Guide for the Care and Use of Laboratory Animals (NIH Publications No. 85-23, revised 1996). The animals were maintained on standard mice chow and water *ad libitum*, under a 12/12-hour light/dark cycle and standardized housing conditions before and after operation. The mice were randomly divided into the following four groups: immediate repair group (n = 6; tibial nerve transection and immediate repair); 1-month delay group (n = 10; tibial nerve transection and repair after a 1-month delay); 3-month delay group (n = 20; tibial nerve transection and repair after a 3-month delay); and control group (n = 6; no damage to tibial nerve).

PNI modeling

Denervation of the target muscle

The animals were anesthetized using 1.5% isoflurane (RWD Life Science Co., Shenzhen, China) inhalation. All surgeries were performed on the right tibial nerves, using standard microsurgical techniques under aseptic conditions. First, the tibial nerve, peroneal nerve and sural nerve were exposed and freed by gentle dissection. The right tibial nerves were transected approximately 3 mm distal to the bifurcation point of the sciatic nerve. Second, according to the previously described protocol (Wu et al., 2013), the proximal nerve stump was ligated and embedded into the nearby muscles by 7-0 nylon stitch. The distal nerve stump was straightened and sutured to neighboring muscles with 7-0 nylon to prevent retraction. At the end of the operation, the wound was closed in layers by 5-0 nylon sutures. Buprenorphine hydrochloride injection (Qinghai Pharmaceutical Factory Co. Ltd., Qinghai, China), 0.01 mg/kg, was given subcutaneously once immediately after the surgery and daily in the first 3 postoperative days. Diclofenac sodium (10 mg/L in drinking water; Novartis, Beijing, China) was given by oral administration for the first 7 postoperative days.

Reinnervation of the target muscle

The tibial nerve stumps were re-exposed for secondary anastomosis according to group assignment. The proximal and distal nerve stumps were freed, and the neuroma of the proximal stump and the scar of the distal stump were trimmed. Then, the proximal and distal stumps were inserted 1 mm into a biodegradable chitin conduit (made by our laboratory) using 11-0 nylon stitch. The gap between the proximal and distal stumps was approximately 2 mm. The biodegradable chitin conduit (tube length 4 mm, thickness 0.1 mm, inner diameter 0.6 mm) is a biocompatible and biodegradable artificial nerve graft, as described previously (Yu et al., 2016). No tension at the repair site and the ability to withstand maximal passive exercises with 11-0 sutures without tearing was considered successful nerve repair (Wu et al., 2013). The surgery site was then closed in layers. Buprenorphine hydrochloride injection and diclofenac sodium were given as described above for postoperative pain control.

Electrophysiological examination

After 3 months of reinnervation, a Medlec Synergy electrophysiological system (Oxford Instruments Inc., Oxford, UK) was used to record compound muscle action potentials (CMAPs) from the gastrocnemius muscle in control (n = 6), immediate repair (n = 6), 1-month delay (n = 6), and 3-month delay (n = 7) groups. The repaired nerve was exposed under anesthesia with sodium pentobarbital (Merck, Darmstadt, Germany; 30 mg/kg, intraperitoneal injection) at the experimental side, and then the stimulating bipolar electrode, recording electrode and ground electrode were placed in the proximal nerve trunk, gastrocnemius and thigh muscle, respectively. Rectangular pulses (duration 0.1 ms, intensity 0.06 mA, frequency 5 Hz) were applied to acquire CMAPs.

Osmium tetroxide staining and examination of the tibial nerve

The distal tibial nerves 2 mm distal to the repair site from control (n = 6), immediate repair (n = 6), 1-month delay (n = 6), and 3-month delay (n = 7) groups were obtained after electrophysiological examination to assess nerve regeneration. The nerves were fixed in 1% w/v osmium tetroxide in double distilled water for 12 hours, sequentially dehydrated in 50%, 70%, 90% and 100% ethyl alcohol, and embedded in paraffin. Consecutive 2-μm-thick transverse sections were cut using a microtome (Leica RM2135, Wetzlar, Germany). The nerve sections were mounted onto slides and imaged under a microscope (Leica DM4B with Leica Application Suite X (LAS X) software, Wetzlar, Germany) with a 20× objective to count the number of myelinated axons.

Labeling of MEPs and tissue optical clearing

To observe the structure of regenerating MEPs, Alexa Fluor647-Bungarotoxin (Invitrogen, Carlsbad, NY, USA) was injected through the caudal vein to label MEPs after electrophysiological examination (Chen et al., 2016). First, 1 hour after α-BTX injection (0.3 μg/g), the mice in control (n = 6), immediate repair (n = 6), 1-month delay (n = 6), and 3-month delay (n = 7) groups were perfused transcardially with normal saline solution followed by 4% w/v paraformaldehyde in 0.01 M phosphate-buffered saline. Second, the intact gastrocnemius muscle was dissected and postfixed with 4% paraformaldehyde at 4°C overnight. Third, optical clearing was performed on the postfixed muscle using the 3DISCO technique (Ertürk et al., 2012; Wan et al., 2018). The postfixed muscle was dehydrated sequentially in 50%, 70%, 80% and 100% tetrahydrofuran (Sinopharm Chemical Reagent Co., Ltd., Beijing, China), and then treated with 100% dibenzyl ether (Sigma-Aldrich, St. Louis, MO, USA) to achieve complete transparency. The sample was shaken for 2.5 hours at 4°C during each clearing step.

Confocal microscopy observation

The transparent muscle in control (n = 6), immediate repair (n = 6), 1-month delay (n = 6), and 3-month delay (n = 7)

groups was imaged on a cover glass under an inverted confocal microscope (Zeiss LSM710, Oberkochen, Germany). The fluorescent signals of MEPs were observed with a 647-nm excitation wavelength. Three microscopic fields were randomly selected in every muscle to obtain 40-μm-thick stacks in the Z-axis (1-μm steps) with a 10× objective. The two-dimensional images of MEPs were obtained by maximum-intensity projection (MIP) reconstruction using ImageJ software (National Institutes of Health, Bethesda, MD, USA). The MIP image was used to assess the maturation of MEPs by measuring their area and counting perforations. A perforation is defined as a region where there is no observable α-bungarotoxin staining within the MEP.

Spatial distribution of MEPs

To observe the spatial distribution of MEPs in gastrocnemius muscle, the intact muscles were imaged under a light-sheeting ultramicroscope (LaVisionBioTec, Bielefeld, Germany) equipped with MV PLAPO 2X/0.5 dry objective (W.D. 20 mm). The fluorescence image of MEPs (633 nm) in control (n = 6), immediate repair (n = 6), 1-month delay (n = 6), and 3-month delay (n = 7) groups was captured by light-sheet microscopy. The Z-axis step size was 5 μm. The acquired images were analyzed using Imaris software (Bitplane, Zurich, Switzerland) to reconstruct the spatial distribution of MEPs and count their number. To obtain the cross-sectional images of the gastrocnemius and measure the width of the lamellar clusters, we resampled the image stacks, and the MIP of Z-stacks (thickness = 250 μm) were made with ImageJ. There are four lamellar clusters of MEPs (medial MEP lamella, and lateral MEP lamellae (LML) 1–3) on cross-sections of the gastrocnemius (Yin et al., 2019) (**Figure 1**). For each MEP lamella, to calculate the width, we selected one cross-sectional MIP image of the proximal end, middle portion and distal end of the gastrocnemius. We took the average width of these three images as the MEP lamellar width.

Statistical analysis

SPSS 20.0 software (IBM, Armonk, NY, USA) was used for statistical analysis. One-way analysis of variance followed by the Student-Newman-Keuls test was used for two-group comparison and multi-group comparison, respectively. All data are expressed as mean ± standard deviation (SD), and statistical significance was defined as $P < 0.05$.

Results

General condition of the mice with delayed repair after PNI

There were six mice in the immediate repair group (100% success rate), six in the 1-month delay group (60% success rate) and seven in the 3-month delay group (35% success rate) that had successful repair without tension. All of the mice survived and had a good nutritional status after the second surgery. However, there were varying degrees of muscle atrophy in the right hind limbs of mice in the repair nerve groups.

Electrophysiological examination of the gastrocnemius in mice with delayed repair after PNI

Three months after nerve repair, gastrocnemius CMAPs were recorded in each group. The waveforms in the repair groups (immediate repair, 1-month delay, and 3-month delay) were the same as that in the control group (**Figure 2**). The amplitudes of the gastrocnemius CMAPs were 16.0 ± 1.6, 10.4 ± 1.1, 1.2 ± 0.5 and 28.5 ± 3.1 mV in the immediate repair, 1-month delay, 3-month delay and control groups, respectively. CMAP amplitudes in the four groups were significantly different ($P < 0.05$).

Pathology of the tibial nerve in mice with delayed repair after PNI

Osmium tetroxide staining revealed regenerated myelinated axons in the distal tibial nerve (**Figure 3**). The number of regenerated axons decreased with increasing denervation time. Except for the immediate repair and 1-month delay groups, there were significant differences ($P < 0.05$) in the number of regenerated axons among the groups.

Regeneration of MEPs in the gastrocnemius of mice with delayed repair after PNI

Confocal microscopic images revealed the structure of regenerating MEPs. The shape of MEPs in the gastrocnemius appeared uniformly pretzel-shaped in the immediate repair and control groups, whereas the shapes of the MEPs in the 1-month delay and 3-month delay groups were irregular and the fluorescent signal was heterogeneous (**Figure 4A–D**). The mean area of MEPs in the 3-month delay group was significantly smaller than those in the immediate repair and control groups ($P < 0.05$; **Figure 4E**). There were no differences between the immediate repair and control groups ($P > 0.05$). We also assessed maturation of MEPs by counting perforations in single MEPs, and found significant difference among the four groups ($P < 0.05$; **Figure 4F**). The maturity of MEPs gradually decreased with increasing denervation time.

Spatial distribution of MEPs in the gastrocnemius of mice with delayed repair after PNI

To assess whether delayed repair influences the spatial redistribution of MEPs in gastrocnemius muscle, light-sheet microscopy was used to observe structural changes. Three-dimensional reconstruction (**Additional Video 1**) showed that the regenerated MEPs were also distributed within lamellar clusters after delayed repair (**Figures 5** and **6A–D**). However, the homogeneity of MEPs and lamellar cluster dimensions were changed in the 3-month delay group. The width of the lamellar clusters on cross-sections of the gastrocnemius in the 3-month delay group was larger than in the other three groups ($P < 0.05$). However, there was no difference in width of the lamellar clusters in cross-sections of the gastrocnemius among the immediate repair, 1-month delay and control groups ($P > 0.05$; **Figure 6E**). Moreover, we counted the MEPs in each group. This revealed differences among the four groups ($P < 0.05$; **Figure 6F**). To examine MEP regeneration in the lamellar clusters, we further counted the MEPs per lamellar cluster. As with the number of total MEPs, the number of MEPs per lamellar cluster also gradually declined with increasing denervation time ($P < 0.05$; **Figure 6G**), and the rate of decline was different among the lamellar clusters in the 3-month delay group (**Table 1**).

Table 1 | **The number and ratio of MEPs per lamellar cluster**

Group	Total MEPs in gastrocnemius	MEPs in MML[a]	MEPs in LML1[a]	MEPs in LML2[a]	MEPs in LML3[a]
Immediate repair (n = 6)	11392±499	3393±291(29.8±1.6%)	2377±217(20.1±1.3%)	2285±115(20.1±0.7%)	3337±97(29.3±1.6%)
1-Mon delay (n = 6)	8053±1146	2427±437(30.0±1.4%)	1624±200(20.2±1.0%)	1580±229(19.6±0.9%)	2422±32(20.3±1.1%)
3-Mon delay (n = 4)	2820±251	1114±113(40.0±1.2%)	271±37(9.6±0.6%)	324±42(11.5±1.4%)	1104±99(39.2±0.6%)
Control (n = 6)	13429±971	4000±257(29.8.0±1.1%)	2732±271(20.3.0±1.1%)	2628±160(19.6±1.2%)	4069±471(30.2±1.5%)

[a]Data are expressed as number (ratio) (mean ± SD) and were analyzed by one-way analysis of variance followed by the Student-Newman-Keuls test. LML1: Lateral MEP lamella 1, LML2: lateral MEP lamella 2, LML3: lateral MEP lamella 3; MEP: motor endplate; MML: medial MEP lamella.

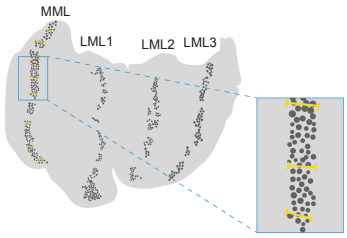

Figure 1 | Schematic diagram of the measurement of the width of MEP lamellar clusters on cross-sections of the gastrocnemius.
Four lamellar clusters of MEPs (MML, LML1, LML2, LML3) are observable in cross-sections of the gastrocnemius. These lamellar cluster are indicated with grey dots. The yellow line represents the width of lamellar clusters. For each MEP lamella, to calculate their width, we selected one cross-sectional MIP image in the proximal, middle and distal ends of the gastrocnemius. We took the average width of these three images as the MEP lamellar width. LML: Lateral motor endplate lamella; MEP: motor endplate; MIP: maximum-intensity projection; MML: medial motor endplate lamella.

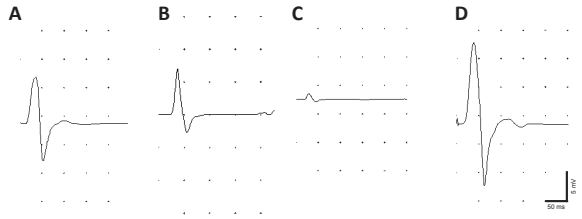

Figure 2 | Electrophysiological examination of gastrocnemius muscles in mice with delayed repair after peripheral nerve injury.
CMAPs of gastrocnemius muscles were recorded 3 months after surgery. (A–D) The waveforms in the immediate repair (A), 1-month delay (B) and 3-month delay (C) groups were the same as in the control group (D). The CMAPs of the gastrocnemius muscle gradually diminished with longer denervation time. The horizontal axis represents duration (bars: 50 ms). The Y-axis represents the voltage (bars: 5 mV). CMAP: Compound muscle action potential.

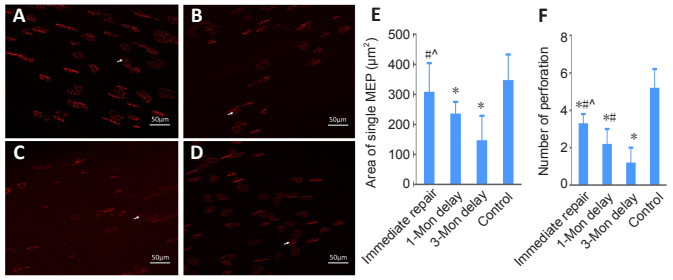

Figure 3 | Osmium tetroxide staining of the regenerated tibial nerve in the gastrocnemius of mice with delayed repair after peripheral nerve injury.
(A–D) Light microscopy images of transverse sections of the tibial nerve in the immediate repair (A), 1-month delay (B), 3-month delay (C) and control (D) groups. The number of regenerated axons was visibly decreased with increased denervation time. Scale bars: 50 μm. (E) Quantitation of the number of regenerated axons. Data are expressed as mean ± SD (n = 6, 6, 7 and 6 in the immediate repair, 1-month delay, 3-month delay and control groups, respectively). *P < 0.05, *vs.* control group; #P < 0.05, *vs.* 3-month delay group; ^P < 0.05, *vs.* 1-month delay group (one-way analysis of variance followed by the Student-Newman-Keuls test).

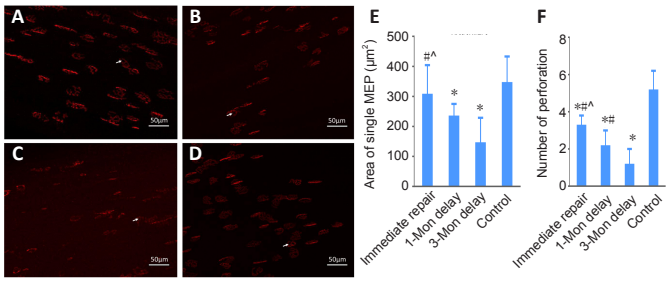

Figure 4 | Confocal microscopy of the MEPs in the gastrocnemius of mice with delayed repair after peripheral nerve injury.
(A–D) MEPs were stained with α-bungarotoxin (red, stained by Alexa Fluor647) and visualized in muscles in the immediate repair (A), 1-month delay (B), 3-month delay (C) and control (D) groups. Regenerated MEPs can be directly visualized after delayed repair. White arrows indicate perforation of MEPs. However, the shape of MEPs in the 1-month delay and 3-month delay groups was irregular compared with those in the immediate repair and control groups. Scale bars: 50 μm. (E) The superficial area of single MEPs in each group. The area is gradually reduced with longer denervation time. (F) The number of perforations of single MEPs in each group. MEP maturation is more severely perturbed in the 1-month delay and 3-month delay groups compared with the immediate repair and control groups. Data are expressed as mean ± SD (n = 6, 6, 7 and 6 in the immediate repair, 1-month delay, 3-month delay and control groups, respectively) *P < 0.05, *vs.* control group; #P < 0.05, *vs.* 3-month delay group; ^P < 0.05, *vs.* 1-month delay group (one-way analysis of variance followed by the Student-Newman-Keuls test). MEP: Motor endplate.

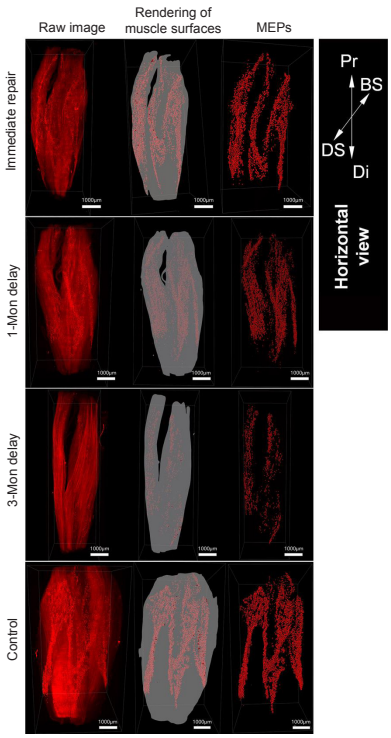

Figure 5 | Three-dimensional reconstruction of MEPs in the gastrocnemius in the different groups of mice with delayed repair after peripheral nerve injury.
The regenerated MEPs are also distributed within lamellar clusters after delayed repair. BS: Bone surface; Di: distal end; DS: dorsal surface; MEP: motor endplate; Pr: proximal end. Scale bars: 1000 μm.

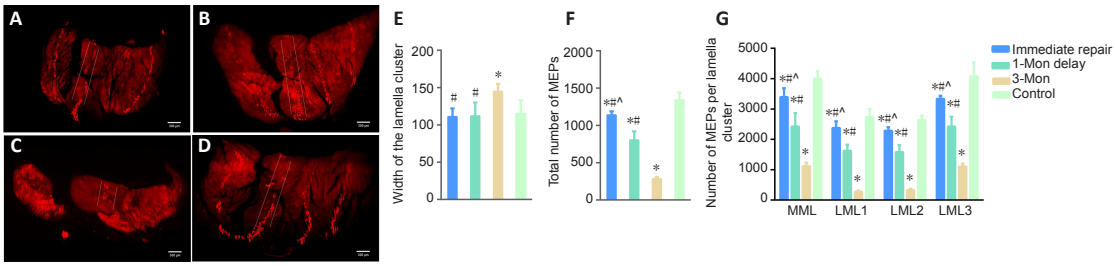

Figure 6 | Cross-sectional images of MEPs in the gastrocnemius in the different groups of mice with delayed repair after peripheral nerve injury.
(A–D) Maximum projections of z-stacks of the cross-sectional images (thickness 250 μm) in muscles in immediate repair (A), 1-month delay (B), 3-month delay (C) and control (D) groups. White lines indicate lamellar MEP clusters. Scale bars: 300 μm. (E) The width of the lamellar cluster. (F) The total number of MEPs. (G) The number of MEPs per lamellar cluster. Data are expressed as mean ± SD (n = 6, 6, 7 and 6 mice in the immediate repair, 1-month delay, 3-month delay and control groups, respectively). *P < 0.05, *vs.* control group; #P < 0.05, *vs.* 3-month delay group; ^P < 0.05, *vs.* 1-month delay group (one-way analysis of variance followed by the Student-Newman-Keuls test). MEP: Motor endplate.

Discussion

In this study, to further explore the regeneration of MEPs after PNI, a delayed tibial nerve repair model was successfully established with a biological conduit small gap sleeve bridging as secondary repair (Zhang et al., 2015). The 52% overall success rate of tension-free direct repair was lower than that reported by Wu et al. (2013). In their study, the Lewis rat sciatic nerve was transected and maintained for 0, 1, 4, 6, 8 or 12 weeks before being repaired through anastomosis. A successful repair was defined when the gap was shorter than 4.0 mm and the stumps could be reapproximated with 10-0 stitches without detachment. We postulated that the lower success rate in our study might be associated with the shorter lengths of the nerves in mouse compared with rat. In this study, we found that delayed repair partially restored motor function in the mice. However, the CMAPs and number of regenerated axons were significantly reduced by prolonged denervation. These data are in accordance with those reported previously (Kobayashi et al., 1997; Jiao et al., 2015).

In this study, a novel and convenient approach combining MEP labeling with the optical clearing technique (Chen et al., 2016) was used to explore the number and spatial distribution of MEPs after delayed repair. The technique is simple and efficiently obtains the 3D distribution of MEPs. However, the technique cannot display the 3D distribution *in vivo* because it requires a series of chemical treatments on intact muscle *in vitro*. A previous study reported a method of labeling and imaging MEPs *in vivo* (Martinez-Pena y Valenzuela et al., 2010). Their method allows observing changes in MEPs *in vivo*, but it only displays superficial MEPs in muscle.

In the present study, we found that regenerated MEPs were also distributed within lamellar clusters after delayed repair. However, the homogeneity of MEPs in the lamellar clusters changed in the 3-month delay group compared with the immediate repair, 1-month delay and control groups. The reason may be that the remaining MEP fragments cannot guide axons accurately after long-term denervation. Previous studies have demonstrated that the arrangement of AChRs in skeletal muscles is important for guiding axons to innervate MEPs and promote the development of neuromuscular junctions in the developmental stage (Flanagan-Steet et al., 2005; Panzer et al., 2005; Kim and Burden, 2008; Jing et al., 2009). However, long-term denervation typically contributes to the degeneration of MEPs (Shyng and Salpeter, 1989; Bezakova et al., 2001), which may disrupt the arrangement of AChRs. In addition, atrophy makes the muscle unable to undergo reinnervation after long-term denervation. The degradation and fibrosis of the distal nerve stumps is another factor that impedes MEP regeneration. After nerve injury, distal myelin sheaths and nerve terminals undergo a series of cellular and molecular biological alterations and gradually cause degeneration (Benito et al., 2017; Gomez-Sanchez et al., 2017). The synthesis of fibrous tissue acts as a barrier to axonal growth and MEP reinnervation (Pellegrino and Spencer, 1985; Virtanen et al., 1992). Distal nerve segments become less conducive to axonal regeneration and cannot provide pathways for regenerated axons to reconnect MEPs effectively after delayed repair (Aydin et al., 2004; Jonsson et al., 2013). Studies show that lipids, especially cholesterol, are important for maintaining the stability of MEPs. However, after denervation, skeletal muscle starts to atrophy, and the lipid content decreases (Bouteloup et al., 2009), which may also contribute to the fragmentation of MEPs. It has been reported that administering simvastatin after nerve injury reduces cholesterol to promote the recovery of neurological function (Xavier et al., 2012; Morishita et al., 2014). Therefore, the effect of cholesterol on MEPs in denervated skeletal muscle remains unclear and needs to be studied systematically. The combination of adverse factors affects the homogeneous distribution of regenerated MEPs. Therefore, to restore the spatial distribution of regenerated MEPs and their number, nerve terminals should be reconnected to the MEPs within 3 months after nerve injury.

In this study, we also found that long-term denervation negatively affects the maturation of regenerated MEPs. Efficient acetylcholine release and receptor binding depends on MEP maturation (Marques et al., 2000; Sleigh et al., 2014a, b), which is important to the functional recovery of target muscles after delayed repair (Miyamaru et al., 2008). The total number of MEPs gradually decreased as denervation time increased. The decline in the maturation and number of MEPs may be a critical causative factor in target muscle dysfunction after PNI.

There are some limitations to this study. For example, the relationship between the spatial distribution of MEPS and functional recovery was not specifically assessed. Additionally, we only investigated delayed repair of less than 3 months after nerve injury. Delayed repair of longer duration may be required to clarify the long-term effects of denervation on regenerated MEPs. Our previous study showed that the distribution of MEPs is constant in mice of different sexes (Buhtz et al., 1989; Yin et al., 2019). In this study, female mice were used because they have smaller muscles than male mice, and thus require less time for tissue optical clearing. Furthermore, the success rate of delayed repair was lower than immediate repair; the longer the time of delayed repair, the lower the success rate. Thus, the numbers of mice in the four groups were not the same; however, this should not have affected the results.

In summary, we investigated the changes in the number and spatial distribution of regenerated MEPs after delayed repair following nerve injury. Our findings show that delayed repair restores the spatial distribution of MEPs, but adversely affects the homogeneity of MEPs and lamellar MEP clusters in mice.

Acknowledgments: *The authors wish to thank Dan Zhu, Ting-Ting Yu and Jian-Yi Xu of the Britton Chance Center for Biomedical Photonics, Wuhan National Laboratory for Optoelectronics, Huazhong University of Science and Technology for their technical support.*
Author contributions: *Study design: XFY and XFZ; experimental implementation: DDL and JD; data analysis: BJ, SH and XYG; paper writing: DDL. All authors approved the final version of the manuscript.*
Conflicts of interest: *The authors declare that the research was conducted in the absence of any commercial or financial relationships that could be construed as a potential conflict of interest.*
Financial support: *This study was supported by the National Natural Science Foundation of China, Nos. 82072162 (to XFY), 81971177; and the Natural Science Foundation of Beijing of China, No. 7192215 (to XFY). The funding sources had no role in study conception and design, data analysis or interpretation, paper writing or deciding to submit this paper for publication.*
Institutional review board statement: *The study was approved by Animals thics Committee of the Peking University People's Hospital (approval No. 2019PHC015) on April 8, 2019.*
Copyright license agreement: *The Copyright License Agreement has been signed by all authors before publication.*
Data sharing statement: *Datasets analyzed during the current study are available from the corresponding author on reasonable request.*
Plagiarism check: *Checked twice by iThenticate.*
Peer review: *Externally peer reviewed.*

Open peer reviewer: *Zoya Katarova, Institute of Experimental Medicine, Hungarian Academy of Sciences, Hungary.*
Additional files:
Additional file 1: *Open peer review report 1.*
Additional Video 1: *3D reconstruction of MEPs in gastrocnemius muscle after delayed reinnervation.*

References

Aydin MA, Mackinnon SE, Gu XM, Kobayashi J, Kuzon WM Jr (2004) Force deficits in skeletal muscle after delayed reinnervation. Plast Reconstr Surg 113:1712-1718.

Benito C, Davis CM, Gomez-Sanchez JA, Turmaine M, Meijer D, Poli V, Mirsky R, Jessen KR (2017) STAT3 controls the long-term survival and phenotype of repair schwann cells during nerve regeneration. J Neurosci 37:4255-4269.

Bezakova G, Rabben I, Sefland I, Fumagalli G, Lømo T (2001) Neural agrin controls acetylcholine receptor stability in skeletal muscle fibers. Proc Natl Acad Sci U S A 98:9924-9929.

Bouteloup C, Desport JC, Clavelou P, Guy N, Derumeaux-Burel H, Ferrier A, Couratier P (2009) Hypermetabolism in ALS patients: an early and persistent phenomenon. J Neurol 256:1236-1242.

Bryndina IG, Shalagina MN, Sekunov AV, Zefirov AL, Petrov AM (2018) Clomipramine counteracts lipid raft disturbance due to short-term muscle disuse. Neurosci Lett 664:1-6.

Buhtz C, Freitag J, Berge G, Pohl G (1989) Mammographic findings following reduction mammaplasty. Zentralbl Chir 114:36-39.

Chao T, Frump D, Lin M, Caiozzo VJ, Mozaffar T, Steward O, Gupta R (2013) Matrix metalloproteinase 3 deletion preserves denervated motor endplates after traumatic nerve injury. Ann Neurol 73:210-223.

Chen W, Yu T, Chen B, Qi Y, Zhang P, Zhu D, Yin X, Jiang B (2016) In vivo injection of α-bungarotoxin to improve the efficiency of motor endplate labeling. Brain Behav 6:e00468.

Ertürk A, Becker K, Jährling N, Mauch CP, Hojer CD, Egen JG, Hellal F, Bradke F, Sheng M, Dodt HU (2012) Three-dimensional imaging of solvent-cleared organs using 3DISCO. Nat Protoc 7:1983-1995.

Flanagan-Steet H, Fox MA, Meyer D, Sanes JR (2005) Neuromuscular synapses can form in vivo by incorporation of initially aneural postsynaptic specializations. Development 132:4471-4481.

Gomez-Sanchez JA, Pilch KS, van der Lans M, Fazal SV, Benito C, Wagstaff LJ, Mirsky R, Jessen KR (2017) After nerve injury, lineage tracing shows that myelin and remak schwann cells elongate extensively and branch to form repair schwann cells, which shorten radically on remyelination. J Neurosci 37:9086-9099.

Höke A (2006) Mechanisms of Disease: what factors limit the success of peripheral nerve regeneration in humans? Nat Clin Pract Neurol 2:448-454.

Jiao H, Yao J, Song Y, Chen Y, Li D, Liu X, Chen X, Lin W, Li Y, Wang X (2015) Morphological proof of nerve regeneration after long-term defects of rat sciatic nerves. Int J Neurosci 125:861-874.

Jing L, Lefebvre JL, Gordon LR, Granato M (2009) Wnt signals organize synaptic prepattern and axon guidance through the zebrafish unplugged/MuSK receptor. Neuron 61:721-733.

Jonsson S, Wiberg R, McGrath AM, Novikov LN, Wiberg M, Novikova LN, Kingham PJ (2013) Effect of delayed peripheral nerve repair on nerve regeneration, Schwann cell function and target muscle recovery. PLoS One 8:e56484.

Kim N, Burden SJ (2008) MuSK controls where motor axons grow and form synapses. Nat Neurosci 11:19-27.

Kobayashi J, Mackinnon SE, Watanabe O, Ball DJ, Gu XM, Hunter DA, Kuzon WM Jr (1997) The effect of duration of muscle denervation on functional recovery in the rat model. Muscle Nerve 20:858-866.

Li L, Xiong WC, Mei L (2018) Neuromuscular junction formation, aging, and disorders. Annu Rev Physiol 80:159-188.

Magill CK, Tong A, Kawamura D, Hayashi A, Hunter DA, Parsadanian A, Mackinnon SE, Myckatyn TM (2007) Reinnervation of the tibialis anterior following sciatic nerve crush injury: a confocal microscopic study in transgenic mice. Exp Neurol 207:64-74.

Marques MJ, Conchello JA, Lichtman JW (2000) From plaque to pretzel: fold formation and acetylcholine receptor loss at the developing neuromuscular junction. J Neurosci 20:3663-3675.

Martinez-Pena y Valenzuela I, Mouslim C, Akaaboune M (2010) Calcium/calmodulin kinase II-dependent acetylcholine receptor cycling at the mammalian neuromuscular junction in vivo. J Neurosci 30:12455-12465.

Miyamaru S, Kumai Y, Ito T, Yumoto E (2008) Effects of long-term denervation on the rat thyroarytenoid muscle. Laryngoscope 118:1318-1323.

Morishita S, Oku H, Horie T, Tonari M, Kida T, Okubo A, Sugiyama T, Takai S, Hara H, Ikeda T (2014) Systemic simvastatin rescues retinal ganglion cells from optic nerve injury possibly through suppression of astroglial NF-κB activation. PLoS One 9:e84387.

Panzer JA, Gibbs SM, Dosch R, Wagner D, Mullins MC, Granato M, Balice-Gordon RJ (2005) Neuromuscular synaptogenesis in wild-type and mutant zebrafish. Dev Biol 285:340-357.

Pellegrino RG, Spencer PS (1985) Schwann cell mitosis in response to regenerating peripheral axons in vivo. Brain Res 341:16-25.

Pisciotta A, Bertoni L, Vallarola A, Bertani G, Mecugni D, Carnevale G (2020) Neural crest derived stem cells from dental pulp and tooth-associated stem cells for peripheral nerve regeneration. Neural Regen Res 15:373-381.

Rotzler S, Schramek H, Brenner HR (1991) Metabolic stabilization of endplate acetylcholine receptors regulated by Ca^{2+} influx associated with muscle activity. Nature 349:337-339.

Shyng SL, Salpeter MM (1989) Degradation rate of acetylcholine receptors inserted into denervated vertebrate neuromuscular junctions. J Cell Biol 108:647-651.

Slater CR (2020) 'Fragmentation' of NMJs: a sign of degeneration or regeneration? A long journey with many junctions. Neuroscience 439:28-40.

Sleigh JN, Burgess RW, Gillingwater TH, Cader MZ (2014a) Morphological analysis of neuromuscular junction development and degeneration in rodent lumbrical muscles. J Neurosci Methods 227:159-165.

Sleigh JN, Grice SJ, Burgess RW, Talbot K, Cader MZ (2014b) Neuromuscular junction maturation defects precede impaired lower motor neuron connectivity in Charcot-Marie-Tooth type 2D mice. Hum Mol Genet 23:2639-2650.

Virtanen P, Tolonen U, Savolainen J, Takala TE (1992) Effect of reinnervation on collagen synthesis in rat skeletal muscle. J Appl Physiol (1985) 72:2069-2074.

Wan P, Zhu J, Xu J, Li Y, Yu T, Zhu D (2018) Evaluation of seven optical clearing methods in mouse brain. Neurophotonics 5:035007.

Wu P, Spinner RJ, Gu Y, Yaszemski MJ, Windebank AJ, Wang H (2013) Delayed repair of the peripheral nerve: a novel model in the rat sciatic nerve. J Neurosci Methods 214:37-44.

Xavier AM, Serafim KG, Higashi DT, Vanat N, Flaiban KK, Siqueira CP, Venâncio EJ, Ramos Sde P (2012) Simvastatin improves morphological and functional recovery of sciatic nerve injury in Wistar rats. Injury 43:284-289.

Yin X, Yu T, Chen B, Xu J, Chen W, Qi Y, Zhang P, Li Y, Kou Y, Ma Y, Han N, Wan P, Luo Q, Zhu D, Jiang B (2019) Spatial distribution of motor endplates and its adaptive change in skeletal muscle. Theranostics 9:734-746.

Yu Y, Zhang P, Han N, Kou Y, Yin X, Jiang B (2016) Collateral development and spinal motor reorganization after nerve injury and repair. Am J Transl Res 8:2897-2911.

Zhang PX, Li-Ya A, Kou YH, Yin XF, Xue F, Han N, Wang TB, Jiang BG (2015) Biological conduit small gap sleeve bridging method for peripheral nerve injury: regeneration law of nerve fibers in the conduit. Neural Regen Res 10:71-78.

Zhang RC, Du WQ, Zhang JY, Yu SX, Lu FZ, Ding HM, Cheng YB, Ren C, Geng D (2021) Mesenchymal stem cell treatment for peripheral nerve injury: a narrative review. Neural Regen Res 16:2170-2176.

P-Reviewers: Katarova Z, Paduraru L; C-Editor: Zhao M; S-Editors: Yu J, Li CH; L-Editors: Patel B, Yu J, Song LP; T-Editor: Jia Y